3. F. Guttler, T. Irngartinger, T. Plakhotnik, A. Renn, U. P. Wild, *Chem. Phys. Lett.* **217**, 393 (1994).
4. E. B. Shera, N. K. Seitzinger, L. M. Davis, R. A. Keller, S. A. Soper, *ibid.* **174**, 553 (1990); M. D. Barnes, K. C. Ng, W. B. Whitten, J. M. Ramsey, *Anal. Chem.* **65**, 2360 (1993).
5. M. Eigen and R. Rigler, *Proc. Natl. Acad. Sci. U.S.A.* **91**, 5740 (1994); S. Nie, D. T. Chiu, R. N. Zare, *Science* **266**, 1018 (1994).
6. E. Betzig and R. J. Chichester, *Science* **262**, 1422 (1993); X. S. Xie and R. C. Dunn, *ibid.* **265**, 361 (1994).
7. W. P. Ambrose, P. M. Goodwin, J. C. Martin, R. A. Keller, *ibid.* **265**, 364 (1994); *Phys. Rev. Lett.* **72**, 160 (1994).
8. J. K. Trautman, J. J. Macklin, L. E. Brus, E. Betzig, *Nature* **369**, 40 (1994); J. J. Macklin, J. K. Trautman, T. D. Harris, L. E. Brus, *Science* **272**, 255 (1996).
9. T. Ha *et al.*, *Proc. Natl. Acad. Sci. U.S.A.* **93**, 6264 (1996).
10. R. A. Keller *et al.*, *Appl. Spectrosc.* **50** (no. 7), 12A (1996); S. Nie and R. N. Zare, *Annu. Rev. Biophys. Biomol. Struct.*, in press.
11. T. Funatsu, Y. Harada, M. Tokunaga, K. Saito, T. Yanagida, *Nature* **374**, 555 (1995).
12. Th. Schmidt, G. J. Schutz, W. Baumgartner, H. J. Gruber, H. Schindler, *Proc. Natl. Acad. Sci. U.S.A.* **93**, 2926 (1996); Q. Xue and E. S. Yeung, *Nature* **373**, 681 (1995); A. Castro, F. R. Fairfield, E. B. Shera, *Anal. Chem.* **65**, 849 (1993); B. B. Haab and R. A. Mathies, *ibid.* **67**, 3253 (1995).
13. F.-R. F. Fan and A. J. Bard, *Science* **267**, 871 (1995); M. M. Collinson and R. M. Wightman, *ibid.* **268**, 1883 (1995).
14. For reviews, see M. Moskovits, *Rev. Mod. Phys.* **57**, 783 (1985); A. Otto, I Mrozek, H. Grabhorn, W. Akemann, *J. Phys. Condens. Matter* **4**, 1143 (1992); G. C. Schatz, *Acc. Chem. Res.* **17**, 370 (1984).
15. A. B. Meyers, P. Tchenio, M. Z. Zgierski, W. E. Moerner, *J. Phys. Chem.* **98**, 10377 (1994); J. Fleury, Ph. Tamarat, B. Lounis, J. Bernard, M. Orrit, *Chem. Phys. Lett.* **236**, 87 (1995).
16. K. Kneipp *et al.*, abstract 24 presented at the 23rd Annual Conference of the Federation of Analytical Chemistry and Spectroscopy Societies, Kansas City, MO, 29 September to 4 October 1996.
17. A 250-μl aliquot of Ag colloid prepared by the procedure of P. C. Lee and D. Meisel [*J. Phys. Chem.* **86**, 3391 (1982)] was incubated with R6G and ~1 mM NaCl in a 1.5-ml plastic microcentrifuge tube. Glass containers should be avoided because of R6G adsorption on glass surfaces. At the electrolyte concentrations used, the Ag colloid was activated, but not aggregated, after an extended incubation time of ~3 hours at room temperature. The amount of free R6G in solution was experimentally determined to be ~20% by centrifugation of the Ag particles and fluorescence measurement of the supernatant solution. This result is in agreement with the calculated value (~10 to 20%) based on the equilibrium binding constant 1.8×10^{-9} M (*19*). Bulk R6G concentrations from 10^{-7} to 10^{-11} M were calibrated by fluorescence measurement in the absence of Ag colloids. The order, speed, and buffer volume of the colloid-analyte mixing process did not make measurable differences, indicating that equilibrium adsorption conditions were reached in our experiment.
18. R. G. Freeman *et al.*, *Science* **267**, 1629 (1995); G. Chumanov, K. Sokolov, B. W. Gregory, T. M. Cotton, *J. Phys. Chem.* **99**, 9466 (1995).
19. P. Hildebrandt and M. Stockburger, *J. Phys. Chem.* **88**, 5935 (1984).
20. In this integrated microscope, ultrasensitive optical imaging and spectroscopy provided molecular information, and AFM resolved the shape and size of individual nanoparticles. The microscope side port was coupled to a high-throughput, single-stage spectrograph and a back-illuminated charge-coupled device (CCD) detector for spectroscopy. The microscope front was attached to a video-rate intensified CCD for wide-field imaging of single nanoparticles with epi- or evanescent-wave laser excitation. A tapping-mode AFM scanning head was mounted directly on the microscope stage for topographic imaging at nanometer-scale resolution. When coupled with a video data acquisition system, this apparatus allowed digital movies to be made of single nanoparticles at 30 frames per second. Detailed instrument diagram and specifications are available upon request.
21. This question can be addressed by using near-field scanning optical microscopy to image nanoparticle aggregates at a resolution of 50 to 100 nm. Recent research shows that both surface and resonance-enhanced Raman spectra can be obtained with a near-field fiber probe in nanometer domains [S. R. Emory and S. Nie, in *International Conference on Raman Spectroscopy*, S. A. Asher and P. B. Stein, Eds. (Wiley, New York, 1996), pp. 1176–1177; S. Webster, D. A. M. Smith, M. W. Ayad, K. Kershaw, D. N. Batchelder, *ibid.*, pp. 1146–1147].
22. H. Jakobi and H. Kuhn, *Ber. Bunsenges. Phys. Chem.* **66**, 46 (1962).
23. K. Kneipp *et al.*, *Phys. Rev. Lett.* **76**, 2444 (1996).
24. J. T. Golab, J. R. Sprague, K. T. Carron, G. C. Schatz, R. P. Van Duyne, *J. Chem. Phys.* **88**, 7942 (1988).
25. W. Li, J. A. Virtanen, R. M. Penner, *J. Phys. Chem.* **96**, 6529 (1992); *ibid.* **98**, 11751 (1994).
26. C. R. Martin, *Science* **266**, 1961 (1994); *Acc. Chem. Res.* **28**, 61 (1995).
27. R. P. Van Duyne, J. C. Hulteen, D. A. Treichel, *J. Chem. Phys.* **99**, 2101 (1993).
28. T. Xiao, Q. Ye, L. Sun, *J. Phys. Chem.*, in press.
29. A. P. Alivisatos, *Science* **271**, 933 (1996); *J. Phys. Chem.* **100**, 13226 (1996).
30. M. Nirmal *et al.*, *Nature* **383**, 802 (1996).
31. S.N. acknowledges the Whitaker Foundation for a Biomedical Engineering Award and the Beckman Foundation for a Beckman Young Investigator Award. This work was supported by Indiana University Startup Funds.

1 November 1996; accepted 17 December 1996

Direct Measurement of Single-Molecule Diffusion and Photodecomposition in Free Solution

Xiao-Hong Xu and Edward S. Yeung*

Continuous monitoring of submillisecond free-solution dynamics of individual rhodamine-6G molecules and 30-base single-stranded DNA tagged with rhodamine was achieved. Fluorescence images were recorded from the same set of isolated molecules excited either through the evanescent field at the quartz-liquid interface or as a thin layer of solution defined by micron-sized wires, giving diffraction-limited resolution of interconnected attoliter volume elements. The single-molecule diffusion coefficients were smaller and the unimolecular photodecomposition lifetimes were longer for the dye-DNA covalent complex as compared with those of the dye molecule itself. Unlike bulk studies, stochastic behavior was found for individual molecules of each type, and smaller diffusion coefficients were observed.

A variety of approaches have recently been demonstrated for single-molecule detection (SMD) (*1*–*9*). SMD is a way to study and characterize detailed physical and chemical properties that allows the testing of fundamental principles and may lead to technological and methodological developments with applications in medicine, biotechnology, and molecular biology (*5*, *8*, *10*). The detection of single molecules in solution has become relatively straightforward. However, continuous monitoring of a single molecule in free solution remains a challenge (*6*–*9*, *11*). We report here that real-time observation of individual rhodamine-6G (R6G) and rhodamine-labeled 30-base single-stranded DNA (ssDNA) (DNA-R6G) (*12*) molecules in water solution can be achieved by the simple combination of an optical microscope and an intensified charge-coupled device (ICCD) camera. Depending on the arrangement, molecular dynamics either at the quartz-liquid interface or in the bulk liquid can be followed with submillisecond time resolution.

To increase the signal-to-noise ratio in SMD, one can reduce the observation volume (*2*, *6*, *13*), thereby increasing the effective concentration of the molecule of interest. Miniaturization helps to isolate individual molecules, allowing the signal to be assigned to distinct entities. However, fixing a small observation volume and allowing a molecule to diffuse into and out of the region requires either statistics (*5*) or deconvolution with respect to the many possible paths (*7*) in order to extract molecular motion and other kinetic information. One must follow the same molecule continuously because assembly of a large number of single-molecule signals for interpretation (*11*) cannot reveal characteristic differences among molecules as opposed to just mapping out the shape of the probability distribution. The data rate is important in free solution because confinement such as that provided by rigid media (*4*), lipid membranes (*14*), or gel matrices (*15*) is not available. These requirements suggest the

Ames Laboratory–U.S. Department of Energy and Department of Chemistry, Iowa State University, Ames, IA 50011, USA.

*To whom correspondence should be addressed.

use of video microscopy (8). A small volume can be defined by a high-resolution microscope objective when a thin layer of solution is imaged (Fig. 1A). The volume can be further reduced by evanescent-wave excitation of the immediate quartz-liquid layer (Fig. 1B). Recent developments in ICCD sensors provide single-photon counting capability for each pixel element. The associated high-speed readout electronics further allows good temporal resolution to be achieved. This combination forms the basis for the present study.

The measurement of single-molecule photodecomposition lifetimes (τ) in the presence of molecular diffusion requires careful experimental design. For a given fluorophor, τ is typically inversely proportional to the excitation power. A lower laser power allows the fluorophor to continue to emit over a longer time, which favors the monitoring of long-lived molecular dynamics. However, the laser power must be high enough to overcome dark counts from the image intensifier. Also, the observation time affects the isolation of fluorophors. Longer observation times allow more (different) molecules to approach the interfacial region (in the evanescent-wave mode) and accumulate greater lateral diffusion distances for each molecule (in the thin-layer mode). Therefore, there is an optimal combination of laser power and exposure time for each excitation geometry, laser wavelength, fluorophor, and concentration.

Histograms of intensities from images acquired from water, 5 nM R6G, and 40 nM R6G show more high-intensity pixels for 5 nM R6G than for water and more for 40 nM than for 5 nM R6G, confirming single-molecule emission. Selection of an appropriate cutoff threshold [>20 electron counts, based on single photoelectron events and taking into account the gain of the intensifier (80×), the transmission of the fiber optics (50%), and the quantum efficiency of the ICCD (50%)] ensures a negligible number of false positive counts. Further discrimination exists because the signal zones registered by single R6G molecules occupy a larger area than those in water (Fig. 2). Because the evanescent-field thickness is approximately equal to one edge of a pixel, each molecule is equally likely to move out of the excitation zone or move to a neighboring pixel every 0.1 ms (*16*). Thus, the R6G zones in Fig. 2B are broadened because of diffusional motion. In water, most of the signal zones (arising from scattering background) occupy fewer than two pixels per side. This confirms the spatial resolution of the optical system. Occasionally we observed larger spots in water at a frequency of occurrence equivalent to $<10^{-11}$ M. These may be attributable to R6G or other fluorescent contaminants.

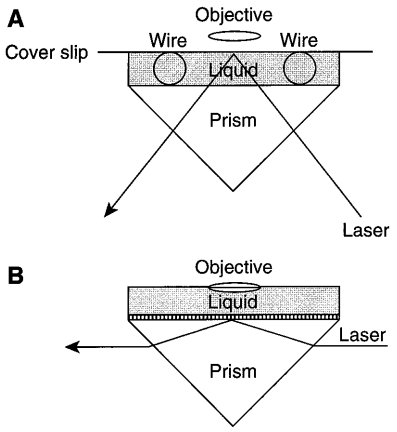

Fig. 1. Schematic diagram of the instrumental setup for SMD. (**A**) Thin-layer mode. (**B**) Evanescent-wave mode. An Ar^+ laser beam is first passed through an equilateral prism to filter out the laser plasma. The unfocused output is directed into a fused-silica right-angle prism located on the microscope stage. This gives a relatively uniform, total internal reflection spot with a diameter of approximately 5 mm. The excitation zone is imaged by a microscope through a 0.08-mm cover slip without immersion oil (A) or through a 100× objective (numerical aperture = 1.3) immersed directly in the solution (B). A mechanical shutter placed in front of the laser beam is used to limit exposure of the sample to the laser. Fluorescence was detected by a 384 × 576 pixel ICCD (Princeton Instruments, ICCD-576 EMG/RB with ST-138 controller) that was mounted at the top entrance of the microscope, facing downward. Each pixel represents a square with 0.2-μm edges, as calibrated by the microscope stage micrometer (0.1 mm per 50 division movements). The image intensifier was coupled to the ICCD through an ordered fiber-optic coupler, and the ICCD element was maintained at −38°C by a thermoelectric cooler. A combination of band-pass and long-pass interference filters was used to collect the signal. The microscope, sample prism, and ICCD were placed inside a box to reduce ambient light and laser scattering. All measurements were made in a darkened room. In (A), the excitation depth was defined by placement of two 4-μm tungsten wires on the prism surface ~50 μm apart. One drop of sample was placed between the wires and a cover slip. The laser penetrates the solution before being totally reflected at the cover slip surface, providing a lower background than epifluorescence arrangements. The total observation region of 3.6×10^{-11} liter can be thought of as being made up of 100,000 independent observation zones (3.6×10^{-16} liter each) defined by the ICCD resolution of 1.5 × 1.5 pixels. Concentrations up to 5 nM can then be used to isolate individual molecules. In (B), the estimated 0.15-μm thickness of the evanescent field defines an observation zone of only 14 al (an attoliter equals 10^{-18} liter). For a fluorophor concentration lower than 10^{-7} M, the molecules will, on average, be isolated from each other within the 100,000 separate observation zones.

Although the spread of the fluorescent spots in the evanescent-wave mode reflects two-dimensional molecular diffusion during exposure, one must follow each molecule continuously to avoid assuming one-to-one correspondence among successive images to define trajectories (*7*, *15*) or confusing photobleaching with molecules leaving the evanescent-wave region (*15*). In the thin-layer mode (Fig. 1A), even molecules moving up and down in the thin-layer solution will be continuously excited and their fluorescence will be recorded.

Figure 3 allows one to determine either the diffusion coefficient (D) or τ when the other is known. The predicted full-width diffusion distances (*17*) $2\bar{\Delta}$, for R6G and DNA-R6G at a 100-ms exposure time, are 75 pixels and 35 pixels, respectively. The much smaller zone sizes in Fig. 3 indicate that every molecule is rapidly bleached or else D is much smaller under these experimental conditions. From the average observed zone widths of 5.4 and 5.1 pixels, we can calculate τ [from the literature value of D (*16*, *17*)] of the R6G and DNA-R6G molecules to be 0.53 and 2.2 ms, respectively (Table 1). Both τ and the integrated intensities are consistent with photodecomposition quantum yields of 10^{-5} to 10^{-6} and a detection efficiency of 0.1%.

To measure D and τ independently and to increase the data rate, we can take ad-

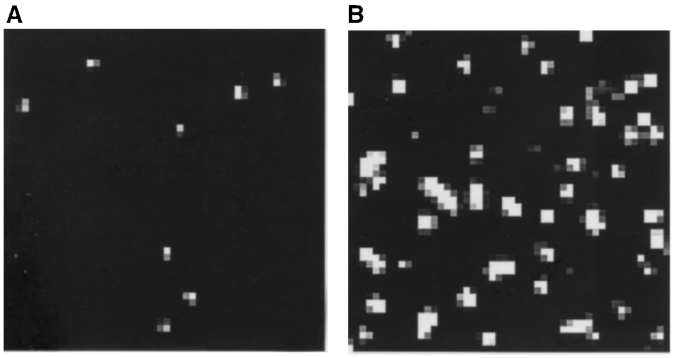

Fig. 2. Subframe images (50 × 50 pixels) of fluorescence from (**A**) water and (**B**) 5 nM R6G. Images were acquired with 50 mW of laser power at 488 nm and a 200-ms exposure time in the evanescent-wave mode (Fig. 1B). The broader zones for R6G depict repeated sampling of fluorescence from molecules undergoing lateral diffusional motion. Excitation occurs only when the molecules approach the evanescent-wave region. The gray scale is from 30 to 50 electron counts.

vantage of a special feature in CCD cameras. During analog-to-digital conversion, each row of the sensor is first shifted upward to a register and digitization proceeds for consecutive pixels in that row. The process is repeated until all rows are read. If the camera shutter is kept open during readout, smearing of the image will occur along the column direction. In Fig. 4, single-molecule emission is clearly distinguishable from the background and is characterized by long tails.

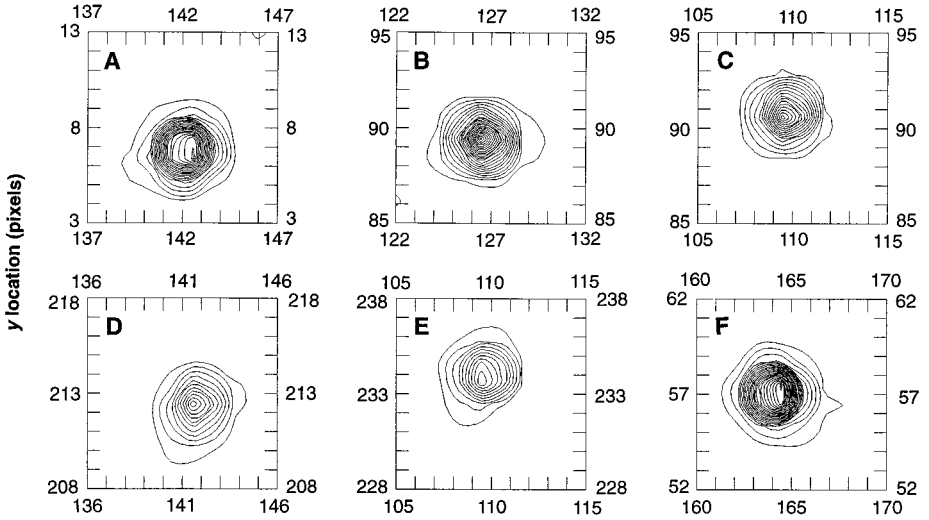

Fig. 3. Contour plots of fluorescence intensities from continuous monitoring of single molecules taken from images of 0.5 nM R6G (**A** through **C**) and 0.5 nM DNA-R6G (**D** through **F**). The different zone widths for R6G reflect different photobleaching lifetimes and different diffusion distances. In (D) through (F), the zones are about the same width as in (A) through (C), despite a slower diffusion coefficient for DNA-R6G. This is due to a substantially longer photobleaching lifetime for DNA-R6G. Images were acquired with 1 mW of laser power at 514 nm and a 100-ms exposure time in the thin-layer mode (Fig. 1A). Contour levels start at 20 electron counts and increase every 7 electron counts.

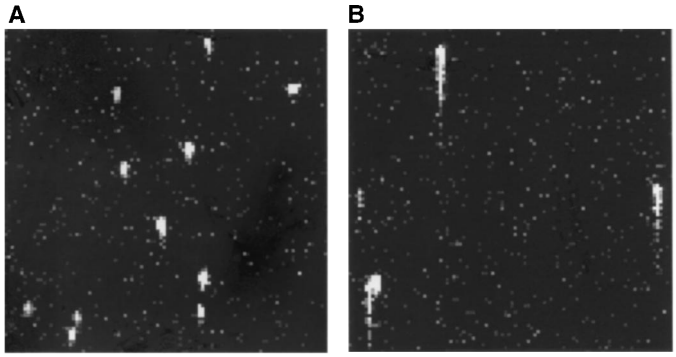

Fig. 4. Subframe images (100 × 100 pixels) of fluorescence continuously recorded from (**A**) 0.5 nM R6G and (**B**) 0.5 nM DNA-R6G. The widths of the heads of the zones correspond to one-dimensional diffusion during the 3.25-ms static exposure. The lengths of the zones are direct measures of the photobleaching lifetimes clocked by the shift rate of the camera. Images were acquired with 1 mW of laser power at 514 nm in the thin-layer mode (Fig. 1A). The shutters were forced open during exposure and readout. The gray scale is from 20 to 40 electron counts.

Table 1. Representative single-molecule photodecomposition lifetimes (τ, in milliseconds) and diffusion coefficients (D, 10^{-7} cm^2 s^{-1}) in free solution.

Molecule	1	2	3	4	5	6	7	8
				Normal images				
τ_1 (R6G)*	0.45	0.64	0.45	0.45	0.88	0.45	0.64	0.29
τ_1 (DNA-R6G)*	1.3	2.0	1.3	2.9	2.0	4.0	2.0	2.0
				Open-shutter images				
D_2 (R6G)†	3.9	5.5	3.9	2.5	3.9	3.9	4.2	4.2
D_2 (DNA-R6G)†	2.5	1.4	1.4	3.9	1.4	3.9	2.5	2.5
τ_2 (R6G)‡	3.6	3.7	4.0	4.3	3.7	3.6	3.6	3.7
τ_2 (DNA-R6G)‡	5.1	7.9	4.8	3.6	4.5	4.0	4.3	3.9

*From Fig. 3, assuming $D = 2.8 \times 10^{-6}$ cm^2 s^{-1} and 6.2×10^{-7} cm^2 s^{-1} for R6G and DNA-R6G, respectively. †From Fig. 4 through direct measurement of the zone width w during the 3.25-ms static exposure. ‡From Fig. 4; direct clocking through the measured tail length after correcting for diffusion distance as measured by the zone width w (from † above). If the total length of the spot is l pixels, the first-order corrected tail length is $(l - w)$ pixels, giving an additional lifetime (beyond 3.25 ms) of 0.377 $(l - w)$ ms and an additional diffusional distance of w $(l - w)$ 0.377/3.25 pixels.

The heads of the spots are wider than the tails (Fig. 4), reflecting molecular diffusion in the row direction during static exposure. This provides an independent means of measuring D and τ (Table 1). There is also diffusion along the column direction. Our ICCD has a digitization rate of 500 kHz and a shift time of 15 μs per row. The time interval between each pixel in a column (for subframes 181 pixels wide) is therefore 0.377 ms. There is also a 3.25-ms exposure time before readout is initiated. So $\tau = [3.25 + 0.377n]$ ms, where n is the tail length in pixels after correction for longitudinal diffusion.

Stochastic behavior in both D and τ is clearly evident in Table 1. D measured directly (Table 1) is, respectively, seven times and 2.6 times smaller for R6G and DNA-R6G as compared with literature values (*7*, *17*), and τ measured directly (Fig. 4) is seven times and 2.1 times longer than predicted from spot sizes (Fig. 3). Our results are thus internally consistent. This implies that in micron-sized domains, bulk values for D no longer apply (*7*, *15*). Because DNA-R6G is highly negatively charged compared to R6G, the deviation of D from bulk values is less near the negatively charged quartz surface. On average, DNA-R6G shows a slightly longer τ (4.6 ± 1.4 versus 3.8 ± 0.3 ms) and an obviously smaller D (2.4 ± 0.5 versus 4.0 ± 0.4 × 10^{-7} cm^2 s^{-1}) as compared with R6G. The larger size of DNA-R6G accounts for the smaller D. Binding to ssDNA can increase τ for rhodamine by stabilizing the excited state (*7*, *18*).

The direct measurement of molecular diffusion coefficients and unimolecular photodecomposition rates for single fluorophors in free solution allows determination of characteristics of each molecule (*19*), not just the population average. The experiments described here are relatively easy to do because the key components are standard items in commercial product lines. In the evanescent-field mode, phenomena on surfaces—such as chromatographic interactions, catalytic surfaces, sensor systems, DNA hybridization, and immunological binding—can be studied at the single-molecule level (*8*). In the thin-layer mode, biomolecular reactions in solution can be followed one step at a time when a fluorophor is being created or destroyed during the reaction. The latter will be reflected as a decrease in the measured lifetime as compared with photobleaching. By synchroniz-

ing observations with the initiation of a reaction [for example, temperature jump and photochemical or electrochemical (*9*, *11*) generation of a reactant], one can follow each molecule as it reacts to see how confined spaces and low concentrations affect reaction rates and equilibrium in order to compare those measurements with macroscopic measurements. The temporal resolution of the open-shutter experiment can be further improved with higher speed A/D cameras (4 MHz is commercially available) or by imaging narrow subframes. If the frame rate is increased to >10 kHz (*16*), then movies can be taken to construct trajectories (*14*, *15*) in free solutions.

REFERENCES AND NOTES

1. B. Rotman, *Biochemistry* **47**, 1981 (1961); Q. Xue and E. S. Yeung, *Nature* **373**, 681 (1995).
2. N. J. Dovichi, J. C. Martin, J. H. Jett, R. A. Keller, *Science* **219**, 845 (1983).
3. W. B. Whitten and J. M. Ramsey, *Anal. Chem.* **63**, 1027 (1991).
4. E. Betzig and R. J. Chichester, *Science* **262**, 1422 (1993); J. J. Macklin, J. K. Trautman, T. D. Harris, L. E. Brus, *ibid.* **272**, 255 (1996).
5. M. Eigen and R. Rigler, *Proc. Natl. Acad. Sci. U.S.A.* **91**, 5740 (1994).
6. S. B. Smith, P. K. Aldridge, J. B. Callis, *Science* **243**, 203 (1989); A. Castro, F. R. Fairfield, E. B. Shera, *Anal. Chem.* **65**, 849 (1993); Y.-H. Lee, R. G. Maus, B. W. Smith, J. D. Winefordner, *ibid.* **66**, 4142 (1994); M. D. Barnes, W. B. Whitten, J. M. Ramsey, *ibid.* **67**, 418A (1995).
7. S. Nie, D. T. Chiu, R. N. Zare, *Anal. Chem.* **67**, 2849 (1995); U. Mets and R. Rigler, *J. Fluorescence* **4**, 259 (1994).
8. T. Funatsu, Y. Harada, M. Tokunaga, K. Saito, T. Yanagida, *Nature* **374**, 555 (1995); R. D. Vale *et al*., *ibid.* **380**, 451 (1996).
9. F.-R. F. Fan and A. J. Bard, *Science* **267**, 871 (1995).
10. J. H. Jett *et al*., *J. Biomol. Struct. Dyn.* **7**, 301 (1989).
11. M. M. Collinson and R. M. Wightman, *Science* **268**, 1883 (1995).
12. Carboxy-rhodamine-6G (absorption maximum = 550 nm) was used to label a 30-base ssDNA to produce 5′-rhod-GAAAA,TGTGC,TGACC,GGACA,TGAAA,ATGAG-3′ (DNA-R6G) with a molecular mass of 9773 g/mol. R6G (laser grade, ACROS, Trenton, NJ) and DNA-R6G (Baron Biotech, Milford, CT) were used without further purification. All solutions were prepared with deionized water from a Millipore Milli-Q system and then carefully filtered three times through a 0.22-μm filter (Costar, Cambridge, MA).
13. R. A. Mathies and K. Peck, *Anal. Chem.* **62**, 1786 (1990); S. A. Soper *et al*., *ibid.* **63**, 432 (1991); K. Ng, W. B. Whitten, S. Arnold, J. M. Ramsey, *ibid.* **64**, 2914 (1992).
14. T. Schmidt, G. J. Schutz, W. Baumgartner, H. J. Gruber, H. Schindler, *Proc. Natl. Acad. Sci. U.S.A.* **93**, 2926 (1996).
15. After submission of our work, a related paper appeared [R. M. Dickson, D. J. Norris, Y.-L. Tzeng, W. E. Moerner, *Science* **274**, 966 (1996)]. By correlating the fluorescence spots in consecutive images, Dickson *et al*. followed molecular diffusional motion by constructing trajectories of motion. The images were recorded every 0.7 s, so only highly restricted motion, such as that found in certain pores of gel matrices, could be studied. Because evanescent-wave excitation was used, the observed intensities could be used to estimate the *z* position of the molecule, assuming there were no orientational or environmental effects on the spectroscopic properties. The molecules were not monitored continuously, so photobleaching could not be distinguished from movement away from the evanescent field. To study dynamics in free solution, as is demonstrated in our study, one needs a faster temporal response, the ability to observe the molecules continuously, and a way to decouple diffusion from photodecomposition.
16. The diffusion time *t* of R6G ($D_{R6G} = 2.8 \times 10^{-6}$ cm^2 s^{-1}) (*7*) for a diffusion distance $\bar{\Delta}$ of 0.2 μm (one edge of a pixel) is 0.1 ms based on random-walk theory, $\bar{\Delta} = (2Dt)^{1/2}$ [L. B. Anderson and C. N. Reilley, *J. Chem. Educ.* **44**, 9 (1967)].
17. The diffusion coefficient of DNA-R6G ($D = 6.2 \times 10^{-7}$ cm^2 s^{-1}) can be estimated from the diffusion coefficient of R6G ($D = 2.8 \times 10^{-6}$ cm^2 s^{-1}) (*7*), based on the mass change, by use of the Stokes-Einstein equation [P. W. Atkins, *Phys. Chem.* (Freeman, San Francisco, CA, 1982), pp. 823–905].
18. J. Tellinghuisen, P. M. Goodwin, W. P. Ambrose, J. C. Martin, R. A. Keller, *Anal. Chem.* **66**, 64 (1994).
19. J. Wang and P. Wolynes, *Phys. Rev. Lett.* **74**, 4317 (1995).

20. The Ames Laboratory is operated for the U.S. Department of Energy by Iowa State University under contract W-7405-Eng-82. This work was supported by the Director of Energy Research, Office of Basic Energy Sciences, Division of Chemical Sciences.

28 October 1996; accepted 7 January 1997

Mass Survival of Birds Across the Cretaceous-Tertiary Boundary: Molecular Evidence

Alan Cooper* and David Penny

The extent of terrestrial vertebrate extinctions at the end of the Cretaceous is poorly understood, and estimates have ranged from a mass extinction to limited extinctions of specific groups. Molecular and paleontological data demonstrate that modern bird orders started diverging in the Early Cretaceous; at least 22 avian lineages of modern birds cross the Cretaceous-Tertiary boundary. Data for several other terrestrial vertebrate groups indicate a similar pattern of survival and, taken together, favor incremental changes during a Cretaceous diversification of birds and mammals rather than an explosive radiation in the Early Tertiary.

The Cretaceous-Tertiary (K-T) boundary, 65 million years ago (Ma), was a key episode in recent vertebrate history, marking the end of the dinosaur era and the rise to predominance of mammalian and avian taxa. This boundary is associated with both an extraterrestrial impact directly at the boundary and periods of flood-basalt volcanism (*1*). The biological consequences of these physical events are poorly understood and controversial (*2*), and several hypotheses have emerged in the absence of direct biological data.

It has been generally thought that Cretaceous avian and mammalian lineages also suffered a mass extinction and that a period of rapid adaptive radiation followed in the Tertiary from a few, or perhaps only a single, surviving lineage (*3*). Alternative hypotheses are that most modern avian (*4*) and mammalian orders survived the K-T boundary or that several lineages survived, perhaps on different continents. The last hypothesis is supported by molecular studies indicating that there are a few deep divergences in small sets of both birds and mammals (*5*, *6*). To further analyze this issue, we combined paleontological and molecular data to examine the K-T boundary extinctions and estimate the times of divergence of modern avian orders.

Molecular data alone cannot be used to determine the extent of extinctions, but, by inverting the question and estimating the number of modern avian and mammalian lineages that survived the K-T boundary, it is possible to estimate some of the biological consequences of the physical events at the boundary. We used early Tertiary fossil records of seven avian orders (Fig. 1) together with DNA sequences from mitochondrial and nuclear genes of a wide variety of avian taxa (*7*) to obtain a minimal estimate of the number of extant avian lineages that crossed the K-T boundary. We obtained a total of 42 sequences (*8*) from a 390–base pair (bp) region of the mitochondrial ribosomal small subunit RNA (12*S*) for 16 avian orders and 16 sequences (*9*) of a 600-bp region of the single-copy nuclear c-*mos* proto-oncogene (*10*) for 10 avian orders (*11*). We concentrated on groups for which Early Tertiary fossil dates were available (Fig. 1).

Our primary method for estimating the divergence times of avian orders is by a quartet method that works in two stages. In the first step, DNA sequences are compared from pairs of related birds for which fossils provide a minimum divergence time (*12*). Pairs must be selected with care so that

A. Cooper, School of Biological Sciences, Victoria University of Wellington, PO Box 600, Wellington, New Zealand, and Molecular Genetics Laboratory, National Zoological Park, Smithsonian Institution, Washington, DC 20008, USA.
D. Penny, School of Biological Sciences, Massey University, PO Box 11222, Palmerston North, New Zealand.

*To whom correspondence should be addressed at Department of Biological Anthropology, Oxford University, Oxford OX2 6QS, UK. E-mail: alan.cooper@bioanth.ox.ac.uk